## PAPER

# Atomic layer deposition of CoF$_2$, NiF$_2$ and HoF$_3$ thin films

Elisa Atosuo, [ID] *[a] Miia Mäntymäki, [ID] [a] Leevi Pesonen,[a] Kenichiro Mizohata,[b] Timo Hatanpää, [ID] [a] Markku Leskelä [ID] [a] and Mikko Ritala [ID] *[a]

The present study describes atomic layer deposition (ALD) processes and characterization of CoF$_2$, NiF$_2$, and HoF$_3$ thin films. For CoF$_2$ deposition CoCl$_2$(TMEDA) (TMEDA = $N,N,N',N'$-tetramethylethylenediamine) and NH$_4$F were used as precursors. CoF$_2$ deposition was studied at 180–275 °C, resulting in a growth per cycle (GPC) of 0.7 to 1.2 Å. All the films consist of tetragonal CoF$_2$ according to XRD. The impurity contents were measured with ToF-ERDA and less than 1 at% of N and Cl were detected in the films, indicating effective reactions. In addition, the F/Co ratio is close to 2 as measured by the same method. The saturation of the GPC with respect to precursor pulses and purges was verified at 250 °C. The common feature of ALD metal fluoride films – remarkable roughness – is encountered also in this process. However, the films became smoother as the deposition temperature was increased. CoF$_2$ deposition was also demonstrated on graphite substrates. NiF$_2$ deposition was studied at 210–250 °C by using Ni(thd)$_2$ and TaF$_5$ or a new fluoride source NbF$_5$ as the precursors. Tetragonal NiF$_2$ was obtained, but the oxygen and hydrogen contents in the films were remarkable, up to ~11 at%, as measured by ToF-ERDA. This was observed also when the films were *in situ* capped with YF$_3$. NbF$_5$ was shown to be a potential fluoride precursor by combining it with Ho(thd)$_3$ to deposit HoF$_3$ films. Orthorhombic HoF$_3$ was obtained at deposition temperatures of 200–275 °C. The films deposited at 235–275 °C are pure, and the Nb contents in films deposited at 250 and 275 °C are only 0.21 and 0.15 at%. The main impurity in both films is oxygen, but the contents are only 1.5 and 1.6 at%. The saturation of the GPC with respect to precursor pulses was verified at 250 °C. The GPC is ~1 Å.

## Introduction

Lithium-ion batteries (LIBs) have been considered as the best choice for challenging energy storage, such as transport, due to their good gravimetric and volumetric energy densities, long cycle life and relatively low cost. To make the most of the LIB technology, research is now focusing on, *e.g.*, 3D solid-state batteries. The performance of 3D solid-state batteries can be improved by developing new cathode materials which have higher capacities than the currently used intercalation transition metal oxides.

One of the active cathode research topics has been transition metal fluorides. They are potential cathode materials for both Li and Na-based battery systems and surpass the commonly used metal oxides in energy densities. The operation principle of transition metal fluoride cathodes is based on conversion reactions with lithium ions. Compared to the conventional layered intercalation oxide cathodes, transition metal fluorides can provide higher capacities due to more transferring electrons per one transition metal ion. In addition, the conversion reactions go to completion, as opposite to the intercalation reactions in the layered oxides, where typically only a fraction of the redox-active metals can be utilized. A selection of conversion cathode materials, such as FeF$_2$, FeF$_3$, CoF$_2$, CoF$_3$, NiF$_2$, and CuF$_2$ have been studied.[1]

For the future 3D solid-state batteries, cathode materials are needed in the form of conformal thin films. However, not many methods have been reported for fabricating thin films of the discussed metal fluorides. For cobalt(II) fluoride, for example, only pulsed laser deposition (PLD), thermal evaporation and molecular beam epitaxy (MBE) have been reported.[2–6] To realize complicated structures needed for 3D solid-state batteries, a sophisticated thin film manufacturing method, such as atomic layer deposition (ALD), is needed. ALD is an advanced version of chemical vapor deposition (CVD) technique. The characteristics of ALD are its ability to uniformly coat 3D shapes, easily controllable film thickness, excellent film purity and stoichiometry, reproducibility, and in general lower deposition temperatures compared to the traditional CVD. These features arise from the self-limiting reactions of the gaseous precursors.[7]

[a]*Department of Chemistry, University of Helsinki, Finland.*
*E-mail: elisa.atosuo@helsinki.fi*
[b]*Department of Physics, University of Helsinki, Finland*

Thanks to the advantageous nature of ALD, many battery component materials (electrodes, solid electrolytes, barrier layers, and artificial electrode–electrolyte interface layers) have already been deposited with ALD.[8] These processes include also some metal fluorides, e.g., LiF and $AlF_3$ which can serve as protective layers for the electrodes.[9,10] Common to all the above-listed metal fluoride cathode materials $FeF_2$, $FeF_3$, $CoF_2$, $CoF_3$, $NiF_2$, and $CuF_2$ is that they lack an ALD process.

In this work, an ALD process for $CoF_2$ is reported. $CoF_2$ was deposited by using $CoCl_2(TMEDA)$ (TMEDA = N,N,N′,N′-tetramethylethylenediamine) and $NH_4F$ as precursors. Also deposition of $NiF_2$ was attempted. However, $NiF_2$ deposition was not straightforward with traditional precursor combinations, and film growth was observed only with the combination of Ni(thd)$_2$ (thd = 2,2,6,6-tetramethyl-3,5-heptanedionato) and $TaF_5$ or $NbF_5$. In addition, the hygroscopicity of $NiF_2$ was noticed to cause remarkable issues to the deposition process. Since $NbF_5$ was however identified as a potential fluoride source, we studied its usability in ALD by studying the deposition of a more stable metal fluoride, holmium fluoride. $NbF_5$ was combined with Ho(thd)$_3$ to produce $HoF_3$ films.

## Experimental section

### Film deposition

The films were deposited in an F120 cross-flow reactor (ASM Microchemistry Ltd) using 99.999% nitrogen as carrier and purging gas. In-house synthesized $CoCl_2(TMEDA)$ and Co(thd)$_2$ (Volatec Oy) were used as cobalt precursors. Their sublimation temperatures were 170 and 98–110 °C. The synthesis of the $CoCl_2(TMEDA)$ precursor is presented elsewhere.[11] $NiF_2$ film deposition was studied by using Ni(thd)$_2$ (Volatec Oy) and in-house synthesized $NiCl_2(TMPDA)$ as nickel precursors. The evaporation temperatures were 125 °C for Ni(thd)$_2$ and 157 °C for $NiCl_2(TMPDA)$. The synthesis of the $NiCl_2(TMPDA)$ precursor is presented elsewhere.[12] $HoF_3$ films were deposited with Ho(thd)$_3$ (Volatec Oy) as the holmium precursor. The evaporation temperature was 125 °C.

$NH_4F$ (Sigma-Aldrich, ≥99.99%), $TiF_4$ (Strem, 98%), $TaF_5$ (Alfa Aesar, 99.9%) and $NbF_5$ (abcr GmbH, 99.5%) were used as fluoride precursors. Their sublimation temperatures were 65–67, 135–145, 45 and 40–45 °C, respectively.

The films were mainly deposited on Si(100) substrates with the native oxide. $CoF_2$ deposition was studied also on graphite substrates (99.95% carbon foil from Goodfellow). The films were stored in a desiccator after deposition.

### Film characterization

Thicknesses of the films were measured with a Film Sense FS-1 multiwavelength ellipsometer by fitting the data with a Cauchy model. Also energy dispersive X-ray spectroscopy (EDS) was used for the thickness determination using an Oxford INCA 350 microanalysis system connected to a Hitachi S-4800 field-emission scanning electron microscope (FESEM). The thicknesses were calculated with the GMRFILM program. Some film thicknesses were confirmed with cross-section FESEM.

EDS was used also to confirm the elements present in the films. Prior to the EDS measurements, the films were coated with carbon to increase the conductivity of the films.

Time-of-flight recoil detection analysis (ToF-ERDA) was used to quantitatively determine the stoichiometry of the films and the impurity contents. A 5 MV tandem accelerator at the accelerator laboratory of University of Helsinki was used for measurements. Measurements were done using 35–40 MeV $^{79}$Br or $^{127}$I primary ions and 40° detection angle.

PANalytical X′pert Pro MPD diffractometer in the grazing incidence X-ray diffraction mode (GI-XRD) was used for crystallinity measurements. The diffractograms were analyzed with a PANalytical HighScore plus software (version 4.7).

FESEM and atomic force microscopy (AFM) were used for studying the morphology of the films. A Veeco Multimode V instrument was used for recording the AFM images. Tapping mode images were captured in air using silicon probes with nominal tip radius of 10 nm and nominal spring constant of 5 N m$^{-1}$ (Tap150 from Bruker). Images were flattened to remove artefacts caused by sample tilt and scanner bow. Roughness was calculated as a root-mean-square value ($R_q$). For FESEM imaging, the films were coated with Au/Pd to increase the conductivity of the samples.

Thermodynamic calculations were done with HSC Chemistry 7.1 software (Outokumpu Research Oy).

## Results and discussion

### Cobalt(II) fluoride films

$CoF_2$ deposition was attempted with the combinations of Co(thd)$_2$ (thd = 2,2,6,6-tetramethyl-3,5-heptanedionato) and $NH_4F$, $TiF_4$, $TaF_5$, or $NbF_5$. With $NH_4F$ no film was obtained. With $TiF_4$ the film deposited at 200 °C possibly consisted of $CoF_2$ according to XRD, but for the film deposited at 300 °C XRD showed strongly crystalline $TiF_3$ phase in addition to the possible $CoF_2$ phase. The combinations of Co(thd)$_2$ and $TaF_5$ or $NbF_5$ were briefly studied at the deposition temperature of 250 °C. In both cases $CoF_2$ phase was seen in XRD. However, in the case of $NbF_5$ the film was blurry and contained ~5 at% of Nb according to EDS. In the case of $TaF_5$ the film contained more tantalum than cobalt according to EDS.

$CoF_2$ was successfully deposited by using $CoCl_2(TMEDA)$ (TMEDA = N,N,N′,N′-tetramethylethylenediamine) and $NH_4F$ as precursors. $CoCl_2(TMEDA)$ is a volatile adduct of the extremely low-volatility $CoCl_2$. It was first presented by Väyrynen et al. in an ALD process for cobalt(II) oxide.[11] The neutral adduct ligand TMEDA is assumed to be released during the chemisorption of the molecule on the growth surface. $NH_4F$ in turn decomposes to HF and $NH_3$ inside the ALD reactor upon heating.[13]

The evaporation temperature of $CoCl_2(TMEDA)$ is 170 °C and it has been reported to decompose at 300 °C.[11] The deposition was thus studied at temperatures of 180–300 °C. After

confirming that the precursor combination produces $CoF_2$ films, the saturation of the growth per cycle (GPC) was studied at 250 °C using 1000 cycles. The $NH_4F$ pulse was studied first by keeping the $CoCl_2(TMEDA)$ pulses and purges at 1 s. Soft saturation was observed when 3 s $NH_4F$ pulses were applied (Fig. 1a, black squares). The effect of the $CoCl_2(TMEDA)$ pulses was studied by keeping the $NH_4F$ pulses at 3 s and the purges at 1 s. For $CoCl_2(TMEDA)$ 0.5 s pulses were sufficient to reach saturation (Fig. 1b). Later, however, it was noticed that more uniform films were obtained when the evaporation temperature of $NH_4F$ was increased by a couple of degrees to 67 °C. The saturation of the GPC was studied again by using 1 s $CoCl_2(TMEDA)$ pulses and 4 s purges (Fig. 1a, red triangles). A better saturation curve was achieved, and 3 s $NH_4F$ pulses were sufficient for the saturation. It was also verified that 3 s purges are sufficient (Fig. 1a, blue circle). The GPC is 1.15 Å.

$CoF_2$ films were deposited at 250 °C also with 250, 500, and 1500 cycles to study the linearity of the growth. As seen in Fig. 2, the thickness of the films grows linearly with the increasing cycle number.

Film growth was studied at 180–300 °C. The lowest deposition temperature 180 °C is only 10 °C higher than the evaporation temperature of the metal precursor but results in uniform films. At 300 °C, in turn, very spotty films were obtained, and this temperature was not studied further. The adhesion of the films to the Si substrate was in general good as was tested with the Scotch tape test.

Fig. 3 shows the GPC of the films deposited at different temperatures using 1000 cycles as calculated from ellipsometry and EDS. In general, the EDS and ellipsometry results are in line with each other at high deposition temperatures, whereas at lower temperatures the difference is larger. This might be explained by the large roughness of the films deposited at lower temperatures which complicates the ellipsometry measurements. Nevertheless, as seen in the EDS results, the trend in the GPC is increasing from 180 to 225 °C and the GPC stays approximately constant at 225 and 250 °C. The GPC increases again at 275 °C. The increase could be explained by the onset of the precursor decomposition as $CoCl_2(TMEDA)$ has been reported to decompose at 300 °C and above.



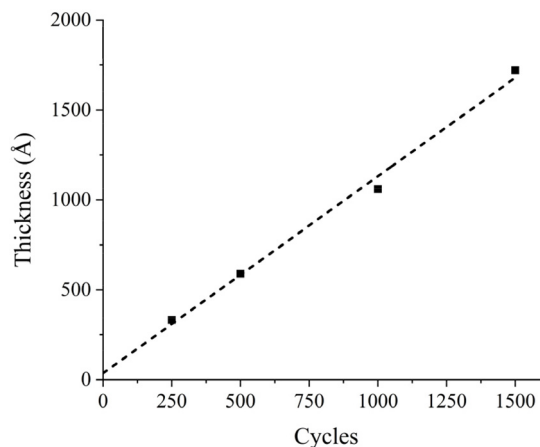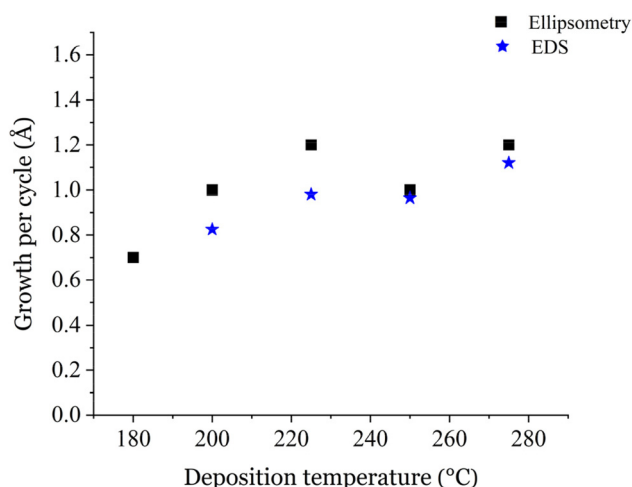**Fig. 2** Thickness of the films as a function of $CoF_2$ deposition cycles.



**Fig. 3** GPC of $CoF_2$ films as a function of the deposition temperature.

All the deposition temperatures (180–300 °C) result in polycrystalline tetragonal $CoF_2$ films as measured by XRD (Fig. 4, ICDD PDF 33-417). There are however differences in the relative diffraction intensities of films deposited at different temp-
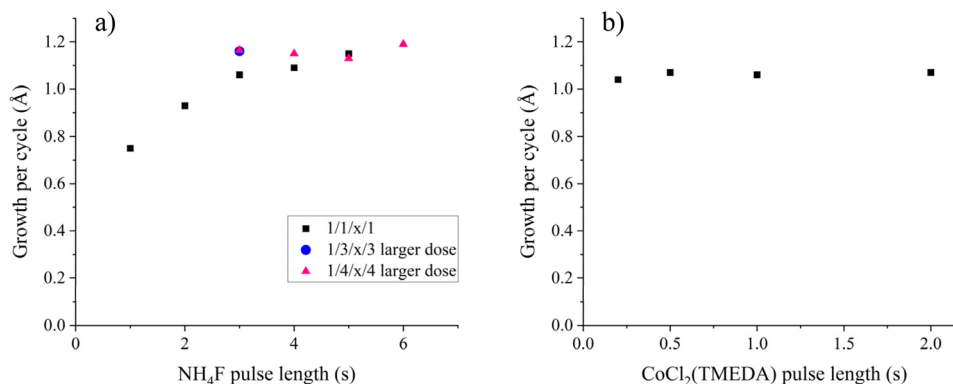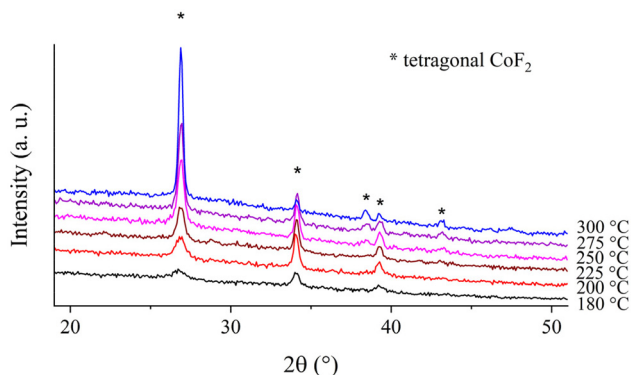


**Fig. 1** GPC as a function of (a) $NH_4F$ and (b) $CoCl_2(TMEDA)$ pulse lengths at 250 °C.

**Fig. 4** GI-XRD of $CoF_2$ films deposited at 180–300 °C. The films are 60–69 nm thick, except the film deposited at 180 °C that is 48 nm thick.

eratures which might indicate different orientations. For a randomly oriented $CoF_2$, the strongest reflection is positioned at $2\theta$ of ~27°. This reflection is seen in our films, and it becomes dominant as the deposition temperature increases. In Fig. 4, the thicknesses of the films are 60–69 nm, except the film deposited at 180 °C which is 48 nm thick. Tetragonal $CoF_2$ has been obtained also with thermal evaporation method.[5]

The composition of the films was studied qualitatively with EDS. In addition to Co, F, and light impurity elements, a small Ni signal was sometimes observed. The possible explanations for this are nickel residues in the reactor or contaminants in the $CoCl_2$ used for the synthesis of $CoCl_2$(TMEDA).

The impurities as well as the stoichiometry were quantitatively measured with ToF-ERDA. Table 1 represents the elemental contents in the films including the surface and Si/$CoF_2$ interface regions. The F/Co ratio 1.9–2.2 is close to the expected 2.0 and thus in line with the XRD results. In addition, the impurity contents are low. For example, the N and Cl contents are less than 1 at% in all the measured films, despite both precursors containing nitrogen. The purest films are those deposited at 225–275 °C, having H, C, N, O, and Cl contents lower than 1 at%. At 250 °C, the total content of these impurities is only 1.15 at%. If some precursor decomposition was to take place already at 275 °C, as discussed earlier, it is not seen as increased impurity contents.

The possible nickel contamination cannot be determined with ToF-ERDA because the similar masses of cobalt and nickel makes their separation impossible. However, because Ni was only occasionally detected with EDS, and the small amount of nickel is not assumed to affect the $CoF_2$ growth, the

nickel content was not determined quantitatively with other methods either.

Based on the XRD and ToF-ERDA results, the precursor combination of $CoCl_2$(TMEDA) and $NH_4F$ seems to work well. To our knowledge, no successful ALD process has been reported in the literature using the precursor combination of a metal chloride and $NH_4F$. These combinations have been previously tested at least for $AlF_3$ and $ZnF_2$, but no film growth was observed.[13] It is interesting to note that $ZnF_2$ films have been deposited by ALD using zinc acetate and $NH_4F$ as precursors.[13] In addition, the $AlCl_3$ + $TiF_4$ process has been shown to work for $AlF_3$ deposition.[14]

Fig. 5 shows FESEM images of films deposited at 200, 250, and 275 °C with 1000 cycles. In the film deposited at 200 °C, rod-shaped grains are seen, and the surface appears rough. At 250 and 275 °C, the grains are larger and merged together, making the film appear more uniform and smoother. The difference in the morphology between the films deposited at 200 and 275 °C is seen also in the cross-section FESEM images (Fig. 6).

Also a thinner film (250 cycles) was deposited at 250 °C and imaged with FESEM (Fig. 5). The morphology resembles the film deposited at 200 °C rather than the thicker film deposited at 250 °C. The film is also not yet continuous. The continuity of thin films was not specifically studied, but at least a film deposited with 500 cycles at the same deposition temperature is continuous.

Due to the morphology of the films, their roughness was assumed to be remarkable. Fig. 7 shows AFM images of films deposited at 200–275 °C. Although the films are only 60–69 nm thick, the root mean square roughnesses ($R_q$) are between 10.9 and 24.7 nm. The largest roughness is measured from the film deposited at the lowest temperature, and the roughness gets smaller as the deposition temperature is increased. This is in line with the FESEM studies. Due to the roughness, the film deposited at the lowest temperature was very difficult to measure with AFM. Note that the z-scales of 200 and 225 °C images are different compared to 250 and 275 °C images.

Since the electronic conductivity of metal fluorides is poor, potential battery materials have been combined, e.g., with carbon to create conducting nanostructures.[15] Therefore, we briefly studied $CoF_2$ deposition also on a graphite substrate. The deposition was done by applying 700 cycles at 250 °C. The precursor pulse lengths were adopted from the $CoF_2$ process on Si, but the purge times were lengthened to 5 s. In FESEM images rod-like features are seen (Fig. 8). According to XRD the film consists of tetragonal $CoF_2$ (Fig. 9).

**Table 1** Elemental contents and stoichiometry as measured by ToF-ERDA for $CoF_2$ films (F/Co ratio 1.9–2.2) deposited with 1000 cycles at different deposition temperatures

| $T_{dep}$ (°C) | Co (at%) | F (at%) | H (at%) | C (at%) | N (at%) | O (at%) | Cl (at%) | F/Co |
|---|---|---|---|---|---|---|---|---|
| 180 | 33 ± 2 | 61 ± 5 | 2.1 ± 0.9 | 0.62 ± 0.12 | 0.11 ± 0.01 | 2.3 ± 0.2 | 0.60 ± 0.08 | 1.9 |
| 200 | 31.6 ± 1.0 | 63 ± 2 | 3 ± 2 | 1.1 ± 0.3 | 0.19 ± 0.08 | 0.98 ± 0.06 | 0.28 ± 0.07 | 2.0 |
| 225 | 32.6 ± 0.8 | 65 ± 2 | 0.9 ± 0.3 | 0.60 ± 0.15 | 0.04 ± 0.00 | 0.79 ± 0.06 | 0.23 ± 0.05 | 2.0 |
| 250 | 31.2 ± 0.6 | 68 ± 2 | 0.25 ± 0.08 | 0.10 ± 0.01 | 0.04 ± 0.00 | 0.63 ± 0.04 | 0.13 ± 0.02 | 2.2 |
| 275 | 33.4 ± 0.6 | 64.1 ± 1.3 | 0.8 ± 0.3 | 0.7 ± 0.3 | 0.03 ± 0.00 | 0.92 ± 0.06 | 0.17 ± 0.03 | 1.9 |

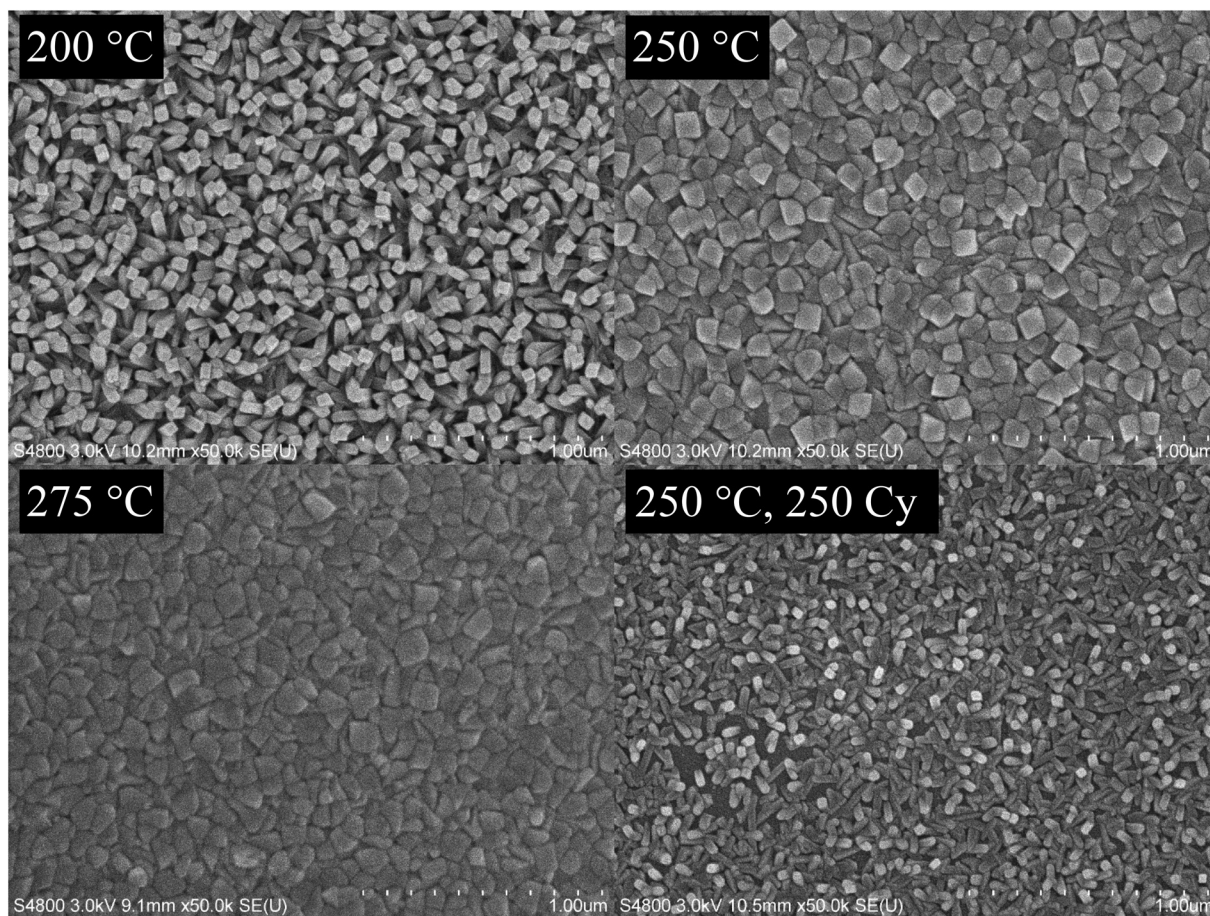**Fig. 5** FESEM images of CoF$_2$ films deposited at 200, 250, and 275 °C with 1000 cycles and at 250 °C with 250 cycles.



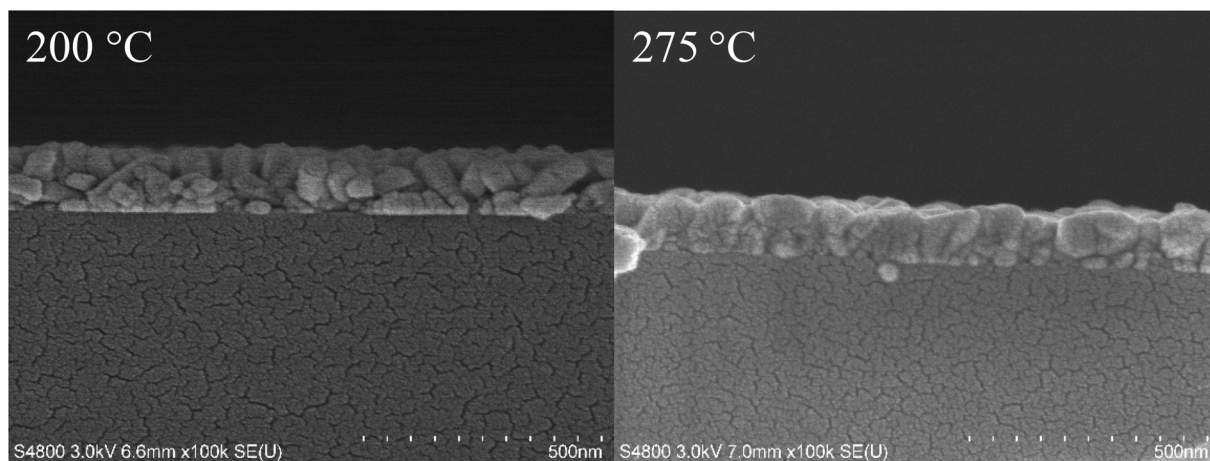**Fig. 6** Cross-section FESEM images of CoF$_2$ films deposited at 200 and 275 °C with 1000 cycles.

### Nickel(II) fluoride films

Nickel(II) fluoride deposition was first attempted with the combination of NiCl$_2$(TMPDA) (TMPDA = $N,N,N',N'$-tetramethyl-1,3-propanediamine)[12] and NH$_4$F, which is similar to the precursor combination used in the successful CoF$_2$ deposition.

No film was obtained, however. Also the more traditional precursor combinations of Ni(thd)$_2$ and NH$_4$F or TiF$_4$ were studied but no film growth was observed.

NiF$_2$ growth was achieved with the combination of Ni(thd)$_2$ and NbF$_5$. The use of NbF$_5$ as the fluoride source in ALD has been mentioned in patents,[16,17] but to our knowledge no
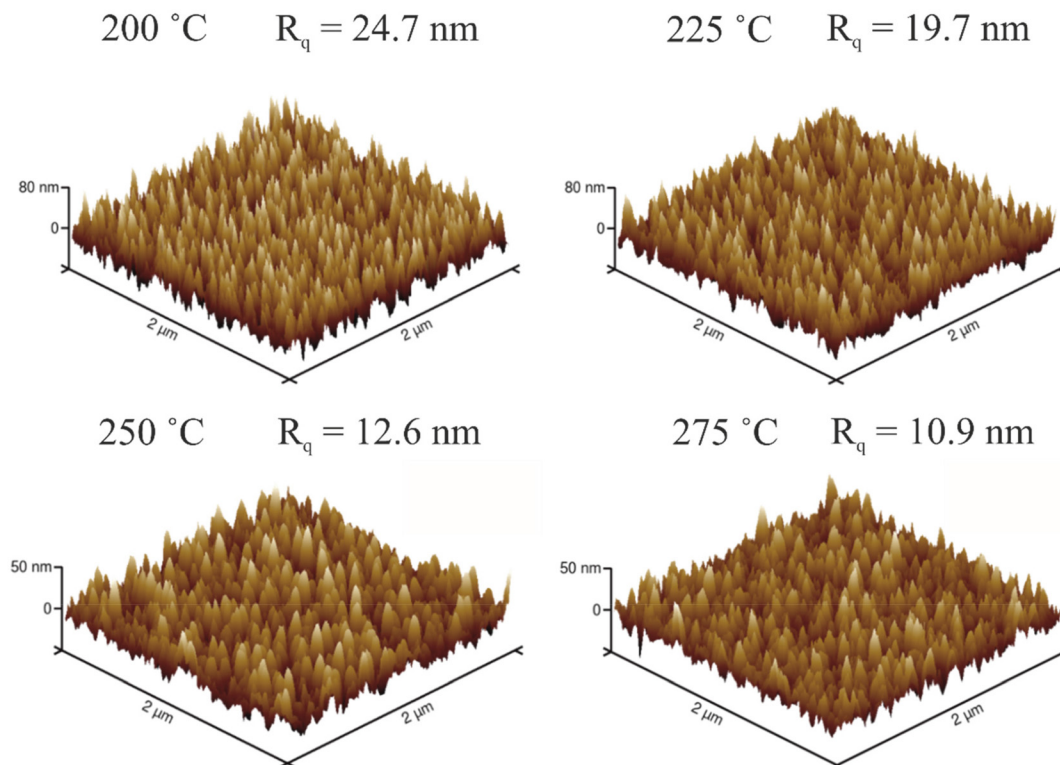
**Fig. 7** AFM images of CoF$_2$ films deposited at 200–275 °C. Note the larger z-scale in 200 and 225 °C images.

process has been published in scientific papers. However, its use as a niobium source in ALD has been reported.[18] NiF$_2$ deposition was studied at 210, 230, and 250 °C. Ni(thd)$_2$ has been reported to decompose at 275 °C,[19] and 250 °C was therefore the highest studied deposition temperature.

According to XRD, all films consist of tetragonal NiF$_2$ (Fig. 10, ICDD PDF file 24-792). The GPC is 0.67 Å at 210 °C and decreases to 0.53 Å at 250 °C. Films deposited with 1500 cycles using 1 s pulses and purges were measured with ToF-ERDA (Table 2). The F/Ni ratio is 2.0–2.2 and thus in line with the XRD results. The hydrogen and oxygen contents are however large in all films, ranging from 8.3 to 10.7 at%. The carbon content is lower, 2.1–3.7 at%. The Nb content is also modest, 3.9–4.4 at%, with no clear trend with the deposition temperature. In addition, small nitrogen contents (0.03–0.07 at%) were found in the films.

The fast erosion of some ALD metal fluoride films during the ToF-ERDA measurement was observed also with the NiF$_2$ films. Therefore, no accurate elemental depth profiles were obtained. To investigate if the hydrogen and oxygen impurities are located on the surface and therefore would be due to post-deposition oxidation, one NiF$_2$ film was capped *in situ* with YF$_3$ film and measured with ToF-ERDA. YF$_3$ was deposited at 250 °C by using Y(thd)$_3$ and TaF$_5$ as precursors. Despite the capping, the hydrogen and oxygen contents are still large indicating that hydrogen and oxygen are probably incorporated into the films already during the deposition. As seen in the depth profiles, hydrogen and oxygen reside clearly in the NiF$_2$ films (Fig. 11a).

NiF$_2$ deposition was briefly studied also by using TaF$_5$ as the fluoride source. The films contained tetragonal NiF$_2$ as measured by XRD (Fig. 10). One film was capped with YF$_3$ and measured with ToF-ERDA. The hydrogen and oxygen contents are similar to the films deposited with NbF$_5$ as the fluoride source. Also in these films hydrogen and oxygen reside clearly in the NiF$_2$ film as seen in the depth profile (Fig. 11b). The large hydrogen and oxygen contents in the NiF$_2$ films deposited with both NbF$_5$ and TaF$_5$ are assumed to result from the hygroscopicity of the NiF$_2$ films.

To investigate the differences in the reactivity of Ni(thd)$_2$ towards NH$_4$F, TiF$_4$, NbF$_5$, and TaF$_5$, thermodynamics were calculated for NiF$_2$ formation in each case using HSC Chemistry software. There are no thermodynamic data for metal thd complexes and therefore corresponding oxides were used as their approximations. In both thd complexes and metal oxides the metal atoms are bonded to oxygen atoms. The calculations were done in bulk form using the following reaction equations:
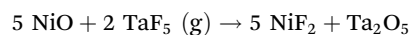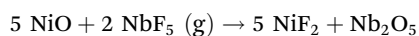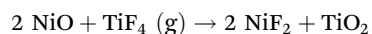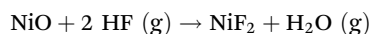
$$NiO + 2\ HF\ (g) \rightarrow NiF_2 + H_2O\ (g)$$

$$2\ NiO + TiF_4\ (g) \rightarrow 2\ NiF_2 + TiO_2$$

$$5\ NiO + 2\ NbF_5\ (g) \rightarrow 5\ NiF_2 + Nb_2O_5$$

$$5\ NiO + 2\ TaF_5\ (g) \rightarrow 5\ NiF_2 + Ta_2O_5$$

Table 3 lists the calculated Gibbs free energies for the formation of one mole of NiF$_2$ at 250 °C. The successful fluoride precursors NbF$_5$ and TaF$_5$ have the most thermodynamically
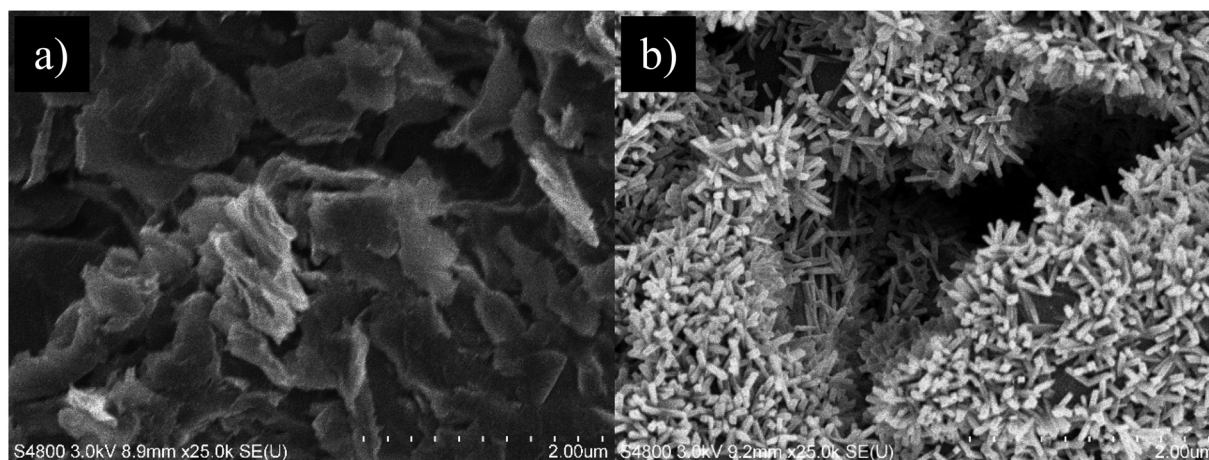
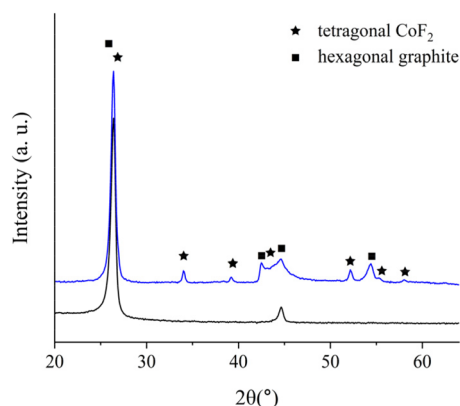**Fig. 8** FESEM images of (a) the bare graphite substrate and (b) a $CoF_2$ film deposited on the graphite substrate.



**Fig. 9** GI-XRD of a bare graphite substrate and a $CoF_2$ film deposited at 250 °C on a graphite substrate.
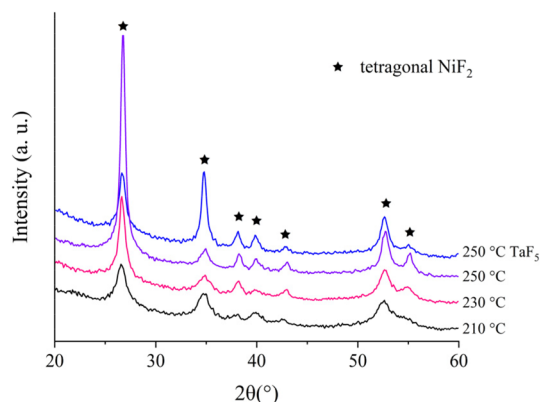


**Fig. 10** GI-XRD of $NiF_2$ films deposited with $NbF_5$ and $TaF_5$ as precursors.

favorable reactions, but there are no noteworthy differences in the Gibbs free energies, especially between $TiF_4$ and $NbF_5$. The reason for obtaining film growth with $NbF_5$ but not with $TiF_4$ is thus not likely explained by thermodynamics alone.

Similar calculations were done also for the formation of one mole of $CoF_2$ at 250 °C from $Co(thd)_2$ and $NH_4F$, $TiF_4$, $NbF_5$, or $TaF_5$ using metal oxides as approximations for metal thd complexes (Table 3). Also in this case $NbF_5$ and $TaF_5$ have the most thermodynamically favorable reactions, but there are no large differences in the Gibbs free energies.

Thermodynamics were calculated also for the reactions $NiCl_2 + 2$ HF (g) $\rightarrow NiF_2 + 2$ HCl (g) and $CoCl_2 + 2$ HF (g) $\rightarrow CoF_2 + 2$ HCl (g). The Gibbs free energy for the formation of one mole of $NiF_2$ at 250 °C is 9.5 kJ whereas for $CoF_2$ it is 2.6 kJ. There is thus no large difference in the favorability of the reactions, although the combination of $CoCl_2(TMEDA) + NH_4F$ resulted in $CoF_2$ growth and the combination of $NiCl_2(TMPDA) + NH_4F$ did not result in $NiF_2$ growth.

Note that the Gibbs free energy for the $CoF_2$ formation is positive for the successful combination of $CoCl_2$ and $NH_4F$ whereas it is negative for the combinations of $Co(thd)_2$ and $NH_4F$, $TiF_4$, $NbF_5$, or $TaF_5$. In the calculations the metal thd complexes have been approximated as metal oxides and in the case of $CoCl_2(TMEDA)$ and $NiCl_2(TMPDA)$ the reacting species is thought to be $CoCl_2$ and $NiCl_2$. Due to these approximations and assumptions the calculations should be used only to roughly compare the favorability of $CoF_2$ and $NiF_2$ formation from similar precursor combinations. Mechanistical studies would be needed to get more insight on the differences in the growth behavior of $NiF_2$ and $CoF_2$. These studies are however out of the scope of this study.

**Holmium fluoride films**

Despite the impurity contents in $NiF_2$ films, $NbF_5$ seemed to be a potential fluoride source, especially because the use of $TiF_4$ and $NH_4F$ as fluoride sources did not produce any film. To show that $NbF_5$ is usable in ALD, we investigated deposition of another metal fluoride—$HoF_3$—by using $NbF_5$ as the fluoride source and $Ho(thd)_3$ as the holmium source. We chose a rare earth ion since they are known to form fluorides easily. Of the rare earth fluorides an ALD process has been reported for

**Table 2** Elemental contents and stoichiometry of $NiF_2$ films (F/Ni ratio 2.0–2.2) deposited with 1500 cycles at different deposition temperatures as measured by ToF-ERDA
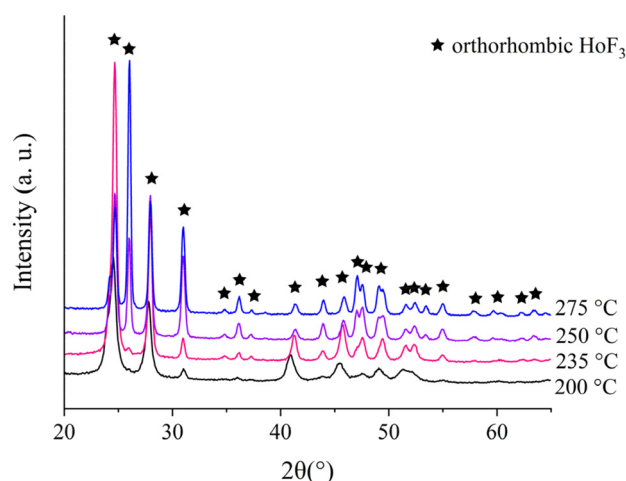
| $T_{dep}$ (°C) | Ni (at%) | F (at%) | H (at%) | C (at%) | N (at%) | O (at%) | Nb (at%) | F/Ni |
|---|---|---|---|---|---|---|---|---|
| 210 | 24.8 ± 0.5 | 49 ± 2 | 10 ± 2 | 3.7 ± 0.8 | 0.03 ± 0.01 | 8.3 ± 0.8 | 4.0 ± 0.2 | 2.0 |
| 230 | 22.8 ± 0.5 | 51 ± 2 | 9.7 ± 1.2 | 3.0 ± 0.8 | 0.07 ± 0.01 | 9.6 ± 0.7 | 3.9 ± 0.1 | 2.2 |
| 250 | 23.5 ± 0.6 | 50 ± 3 | 10 ± 2 | 2.1 ± 0.6 | 0.04 ± 0.01 | 10.7 ± 0.9 | 4.4 ± 0.2 | 2.1 |
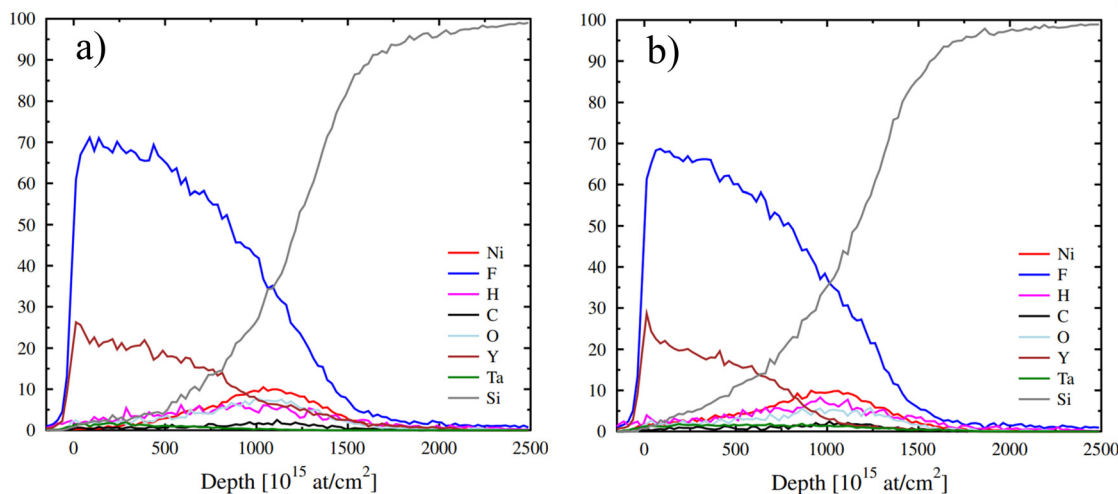


**Fig. 11** Elemental depth profiles of $YF_3$-capped $NiF_2$ films deposited using (a) $NbF_5$ or (b) $TaF_5$ as fluoride source as measured by ToF-ERDA.

**Table 3** Calculated Gibbs free energies for the formation of one mole of $NiF_2$ and $CoF_2$ at 250 °C from different precursors. NiO and CoO serve as approximations for $Ni(thd)_2$ and $Co(thd)_2$

| Metal source | Fluoride source | $\Delta G$ (kJ mol$^{-1}$) |
|---|---|---|
| NiO | HF (from $NH_4F$) | −48 |
| NiO | $TiF_4$ | −64 |
| NiO | $NbF_5$ | −67 |
| NiO | $TaF_5$ | −76 |
| CoO | HF (from $NH_4F$) | −62 |
| CoO | $TiF_4$ | −78 |
| CoO | $NbF_5$ | −82 |
| CoO | $TaF_5$ | −90 |



**Fig. 12** GI-XRD of $HoF_3$ films deposited at 200–275 °C.

$YF_3$, $LaF_3$, and $TbF_3$ using metal thd and $TiF_4$ as precursors[20–22] and for $SmF_3$, $EuF_3$, $GdF_3$, and $TbF_3$ using metal thd and $NH_4F$ as precursors.[23,24] We chose $HoF_3$, a potential material for laser applications,[25] since it has not been deposited earlier by ALD. It is likely that $NbF_5$ is usable also in the deposition of other rare earth fluorides due to the similar nature of the rare earth metals.

The deposition was studied at 200–275 °C. Orthorhombic $HoF_3$ was obtained at all deposition temperatures as measured by XRD (Fig. 12, ICDD PDF 23-284). Saturation of the growth per cycle with respect to pulse lengths was verified at 250 °C (Fig. 13). The $Ho(thd)_3$ pulse was varied between 1 and 3.5 s while keeping the $NbF_5$ pulses at 2 s and purges at 2 s. The GPC saturates around 2 s $Ho(thd)_3$ pulses to ~1 Å (Fig. 13a). The $NbF_5$ pulse length was varied between 0.5 and 3 s while

keeping the $Ho(thd)_3$ pulses at 3 s and purges at 2 s. Saturation of GPC is achieved with 1 s $NbF_5$ pulses (Fig. 13b).

The stoichiometry and elemental contents in the films were measured with ToF-ERDA (Table 4). The F/Ho ratio varies between 2.9 and 3.4 with no clear deposition temperature dependence. The ratio is in line with the XRD results. In the film deposited at 200 °C the impurity contents are quite large. The hydrogen content is the highest, 11.2 at%, followed by the oxygen content (8.1 at%). The Nb content is however modest,
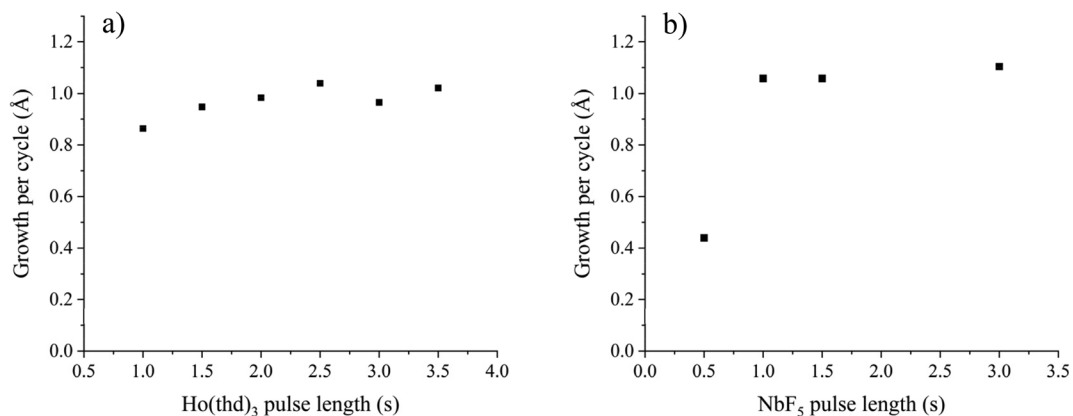
**Fig. 13** GPC as a function of (a) Ho(thd)$_3$ and (b) NbF$_5$ pulse lengths at 250 °C.

**Table 4** Elemental contents and stoichiometry of 84–97 nm HoF$_3$ films (F/Ho ratio 2.9–3.4) deposited at different deposition temperatures as measured by ToF-ERDA

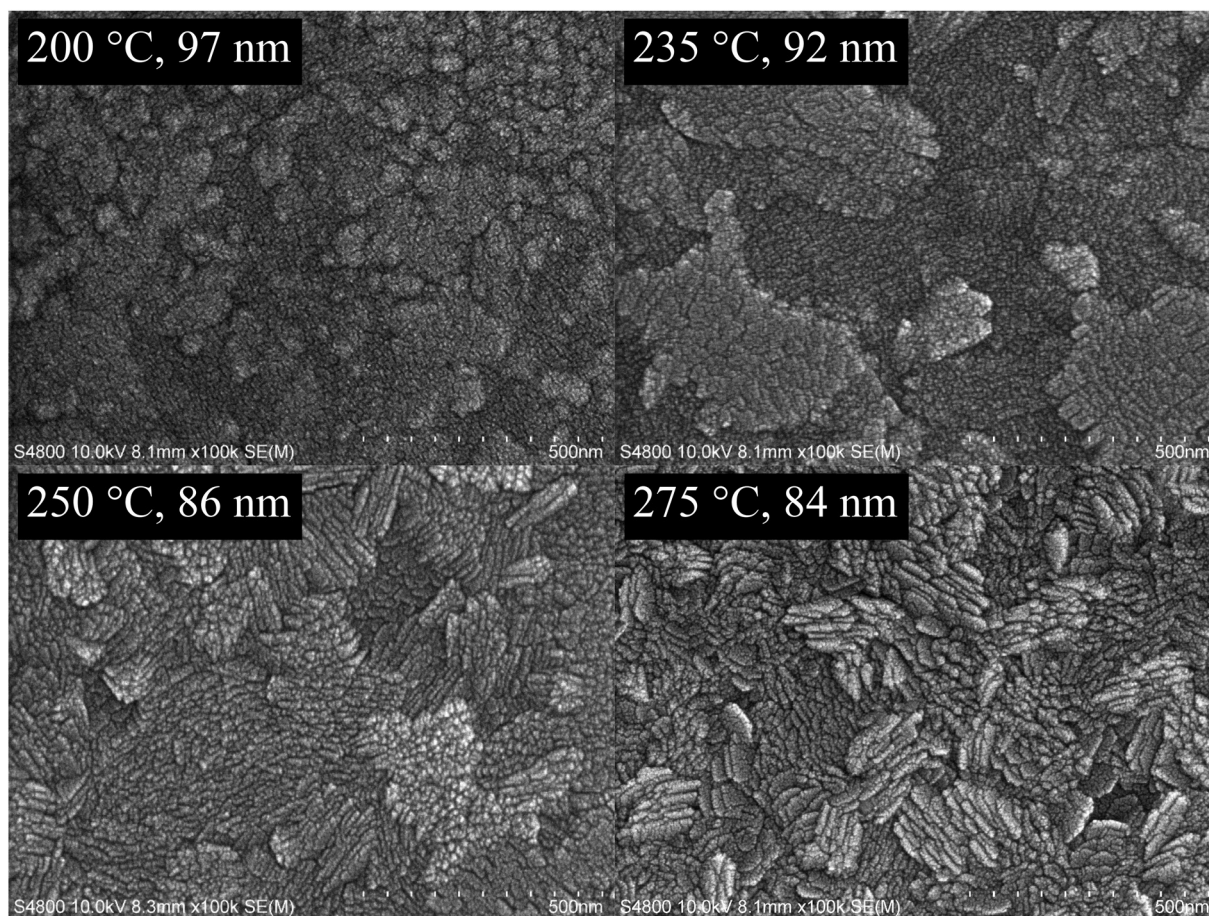| $T_{dep}$ (°C) | Ho (at%) | F (at%) | H (at%) | C (at%) | N (at%) | O (at%) | Nb (at%) | F/Ho |
|---|---|---|---|---|---|---|---|---|
| 200 | 19.2 ± 0.2 | 55.5 ± 1.2 | 11.2 ± 1.1 | 3.7 ± 0.4 | <0.03 | 8.1 ± 0.5 | 2.3 ± 0.2 | 2.9 |
| 235 | 20.5 ± 0.2 | 69.9 ± 1.3 | 4.3 ± 0.6 | 1.2 ± 0.2 | <0.07 | 2.9 ± 0.2 | 1.24 ± 0.12 | 3.4 |
| 250 | 23.4 ± 0.2 | 73.4 ± 1.5 | 1.1 ± 0.3 | 0.43 ± 0.09 | <0.03 | 1.5 ± 0.2 | 0.21 ± 0.04 | 3.1 |
| 275 | 22.8 ± 0.2 | 74.4 ± 1.5 | 0.7 ± 0.2 | 0.30 ± 0.09 | <0.05 | 1.6 ± 0.2 | 0.15 ± 0.03 | 3.3 |



**Fig. 14** FESEM images of HoF$_3$ films deposited at 200–275 °C.

2.3 at%. The films deposited at 235–275 °C are purer, especially the films deposited at 250 and 275 °C. The main impurity in both films is oxygen (1.5 and 1.6 at%). Importantly, the Nb contents are only 0.21 and 0.15 at%.

In FESEM, the 84–97 nm thick films show a lamellar structure, best seen at higher deposition temperatures (Fig. 14). Similar morphology was observed in $YF_3$ films deposited with ALD.[20] The film deposited at 200 °C looks smoother, but the impurity content is also larger than in the other films.

## Conclusions

An ALD process for $CoF_2$ using $CoCl_2$(TMEDA) and $NH_4F$ as precursors was developed. Depositions at 180–275 °C result in tetragonal $CoF_2$. The composition of the film is close to stoichiometric, and the H, C, N, O, and Cl impurities are low as measured by ToF-ERDA. As an example, the total impurity content of these impurities in a $CoF_2$ film deposited at 250 °C is only 1.15 at%. The films grow in rod-like morphology at lower deposition temperatures, whereas at higher deposition temperatures the films are smoother as seen in both SEM and cross-section SEM. Due to the morphology, the films deposited at low temperatures are very rough, *e.g.*, rms roughness is 24.7 nm for a 69 nm film. $CoF_2$ growth on graphite was also briefly studied at a deposition temperature of 250 °C. Tetragonal $CoF_2$ with a rod-like morphology was obtained. $CoF_2$ deposition was also attempted with the precursor combinations of Co(thd)₂ and $NH_4F$, $TiF_4$, $TaF_5$, or $NbF_5$. Either no film growth was seen or there was substantial metal impurity incorporation in the $CoF_2$ films.

$NiF_2$ deposition was studied by using the precursor combinations of Ni(thd)₂ + $NH_4F$, $TiF_4$, $TaF_5$, or $NbF_5$ and $NiCl_2$(TMPDA) + $NH_4F$ which is similar to the precursor combination found successful for the $CoF_2$ deposition. Film growth was observed only when Ni(thd)₂ was combined with $NbF_5$ or $TaF_5$. The films deposited at 210–250 °C by using $NbF_5$ are tetragonal $NiF_2$ according to XRD. However, the films have large hydrogen and oxygen contents as measured by ToF-ERDA. The H and O contents were large in the $NiF_2$ films also when the films were *in situ* capped with $YF_3$, indicating their incorporation into the films already during the deposition. Similar H and O contents were seen also when $TaF_5$ was used as the fluoride source.

The most remarkable difference between $CoF_2$ and $NiF_2$ is the hygroscopicity of $NiF_2$. In addition, $CoCl_2$(TMEDA) and $NH_4F$ resulted in film growth whereas the combination of $NiCl_2$(TMPDA) and $NH_4F$ did not produce any film. There are however no large differences in the Gibbs free energy of the formation of $CoF_2$ and $NiF_2$ from these precursors. With both cobalt and nickel the favorability of the reaction between the metal thd (approximated in calculations as oxides) and a different fluoride source increases in the order $NH_4F$ – $TiF_4$–$NbF_5$–$TaF_5$. There are no large differences in the Gibbs free energies, however. $CoF_2$ formation is in general slightly more favorable than $NiF_2$ formation. In both cases no film was obtained with $NH_4F$ as the fluoride source. In the case of cobalt, a film was obtained with $TiF_4$, $NbF_5$ and $TaF_5$, but severe metal impurity incorporation was seen. In the case of nickel, film was obtained only with $NbF_5$ or $TaF_5$ as the fluoride source. Reaction mechanism studies could reveal the differences in the growth of $CoF_2$ and $NiF_2$, but those are out of the scope of the current paper.

Since $NbF_5$ is a new fluoride source in ALD, we wanted to show that it can be used to deposit good quality ALD metal fluoride films. Thus, we studied the deposition of $HoF_3$ by combining $NbF_5$ with Ho(thd)₃. Orthorhombic $HoF_3$ films were obtained at all the studied deposition temperatures 200–275 °C. The saturation of the GPC with respect to both precursor pulses was achieved at 250 °C. The films deposited at 235–275 °C are pure according to ToF-ERDA, *e.g.*, in the films deposited at 250 and 275 °C the Nb contents are only 0.21 and 0.15 at%. In addition to producing pure $HoF_3$ films, $NbF_5$ produced films with Ni(thd)₂ when no growth was observed with $TiF_4$ or $NH_4F$. $NbF_5$ is thus a potential fluoride source in ALD.

## Conflicts of interest

There are no conflicts of interest to declare.

## Acknowledgements

## References

1 K. Lemoine, A. Hémon-Ribaud, M. Leblanc, J. Lhoste, J.-M. Tarascon and V. Maisonneuve, *Chem. Rev.*, 2022, **122**, 14405–14439.

2 Z.-W. Fu, C.-L. Li, W.-Y. Liu, J. Ma, Y. Wang and Q.-Z. Qin, *J. Electrochem. Soc.*, 2005, **152**, E50.

3 D. Streblechenko and M. R. Scheinfein, *J. Vac. Sci. Technol., A*, 1998, **16**, 1374–1379.

4 M. Malac, M. Schoefield, Y. Zhu and R. Egerton, *J. Appl. Phys.*, 2002, **92**, 1112–1121.

5 P. A. Young, *Thin Solid Films*, 1969, **4**, 25–33.

6 D. Lederman, D. P. Belanger, J. Wang, S.-J. Han, C. Paduani, C. A. Ramos and R. M. Nicklow, *MRS Online Proc. Libr.*, 1993, **313**, 333–338.

7 M. Leskelä and M. Ritala, *Angew. Chem., Int. Ed.*, 2003, **42**, 5548–5554.

8 X. Meng, X.-Q. Yang and X. Sun, *Adv. Mater.*, 2012, **24**, 3589–3615.

9 M. Mäntymäki, J. Hämäläinen, E. Puukilainen, F. Munnik, M. Ritala and M. Leskelä, *Chem. Vap. Deposition*, 2013, **19**, 111–116.

10 Y. Lee, J. W. DuMont, A. S. Cavanagh and S. M. George, *J. Phys. Chem. C*, 2015, **119**, 14185–14194.

11 K. Väyrynen, T. Hatanpää, M. Mattinen, M. Heikkilä, K. Mizohata, K. Meinander, J. Räisänen, M. Ritala and M. Leskelä, *Chem. Mater.*, 2018, **30**, 3499–3507.

12 K. Väyrynen, T. Hatanpää, M. Mattinen, K. Mizohata, K. Meinander, J. Räisänen, J. Link, R. Stern, M. Ritala and M. Leskelä, *Adv. Mater. Interfaces*, 2019, **6**, 1801291.

13 M. Ylilammi and T. Ranta-aho, *J. Electrochem. Soc.*, 1994, **141**, 1278–1284.

14 M. Mäntymäki, M. J. Heikkilä, E. Puukilainen, K. Mizohata, B. Marchand, J. Räisänen, M. Ritala and M. Leskelä, *Chem. Mater.*, 2015, **27**, 604–611.

15 M. Anji Reddy, B. Breitung, V. S. K. Chakravadhanula, C. Wall, M. Engel, C. Kübel, A. K. Powell, H. Hahn and M. Fichtner, *Adv. Energy Mater.*, 2013, **3**, 308–313.

16 J. W. Elam, A. U. Mane and M. Gebhard, US20210254209A1, p. 2021.

17 M. Mäntymäki, M. Ritala and M. Leskelä, US9394609B2, 2016.

18 T. Proslier, J. A. Klug, J. W. Elam, H. Claus, N. G. Becker and M. J. Pellin, *J. Phys. Chem. C*, 2011, **115**, 9477–9485.

19 E. Lindahl, M. Ottosson and J.-O. Carlsson, *Chem. Vap. Deposition*, 2009, **15**, 186–191.

20 T. Pilvi, E. Puukilainen, F. Munnik, M. Leskelä and M. Ritala, *Chem. Vap. Deposition*, 2009, **15**, 27–32.

21 T. Pilvi, E. Puukilainen, K. Arstila, M. Leskelä and M. Ritala, *Chem. Vap. Deposition*, 2008, **14**, 85–91.

22 E. Atosuo, J. Ojala, M. J. Heikkilä, M. Mattinen, K. Mizohata, J. Räisänen, M. Leskelä and M. Ritala, *J. Vac. Sci. Technol., A*, 2021, **39**(2), 022404.

23 P.-A. Hansen, T. Zikmund, T. Yu, J. Nitsche Kvalvik, T. Aarholt, Ø. Prytz, A. Meijerink and O. Nilsen, *Commun. Chem.*, 2020, **3**, 162.

24 E. Atosuo, K. Mizohata, M. Mattinen, M. Mäntymäki, M. Vehkamäki, M. Leskelä and M. Ritala, *J. Vac. Sci. Technol., A*, 2022, **40**(2), 022402.

25 F. Jobin, P. Paradis, Y. Ozan Aydin, T. Boilard, V. Fortin, J.-C. Gauthier, M. Lemieux-Tanguay, S. Magnan-Saucier, L.-C. Michaud, S. Mondor, L.-P. Pleau, L. Talbot, M. Bernier and R. Vallée, *Opt. Express*, 2022, **30**, 8615–8640.